Numerical Simulation of Low-Frequency Current Fluctuations in Lake Michigan[1]

DAVID J. SCHWAB

NOAA Great Lakes Environmental Research Laboratory, Ann Arbor, MI 48104

(Manuscript received 15 April 1983, in final form 25 July 1983)

ABSTRACT

Two simple numerical models have been used to study the low-frequency (<0.6 cpd) current oscillations observed in Lake Michigan in order to learn more about what really limits our ability to simulate currents in large lakes. Both are based on the barotropic vorticity equation with the rigid-lid approximation. One model used observed wind to calculate the time-dependent response of the lake for eight months in 1976. The results agree reasonably well with observed currents, but only in the frequency range corresponding to the maximum energy in the forcing function, approximately 0.125–0.3 cpd. Over this frequency range, peaks in the energy spectrum of the forcing function also occur in both the model response and the observed currents at the same frequencies. At lower and higher frequencies, the model underestimates the observed kinetic energy of the currents. The second model calculates the response of the lake to purely oscillatory wind forcing. From 0.125 to 0.3 cpd, the spatial structure of the response is relatively insensitive to changes in forcing frequency. The response to a north–south oscillatory wind stress resembles a free topographic wave consisting of two counterrotating gyres in the southern basin of the lake, but is more complicated in the northern part. When compared to previous analytic and numerical studies of steady-state circulation, the steady-state (zero frequency) response is found to be consistent with Ekman dynamics for realistic values of linearized bottom stress. The results indicate that the barotropic rigid-lid model can simulate observed current fluctuations only in the 0.125–0.3 cpd frequency range. Over this range, the average response of the lake is nonresonant, showing no peaks in lakewide average kinetic energy. At higher and lower frequencies, baroclinicity and nonlinear effects may have to be included in order to improve the model results.

1. Introduction

Periodic low-frequency (<0.6 cpd) fluctuations in the currents of southern Lake Michigan have been described by Saylor *et al.* (1980) and Huang and Saylor (1982). Similar phenomena in Lake Ontario have been described by Marmorino (1979). The spectral energy density of these oscillations is comparable to the spectral energy density of near-inertial oscillations (Fig. 1). The low-frequency oscillations were predominantly barotropic, with currents in phase above and below the thermocline during the period the lake was stratified. In addition, the rotation of the nearshore currents tended to be clockwise and that of the offshore counterclockwise. These observations are consistent with the structure of the lowest barotropic free oscillation of the second class in a circular paraboloid (Lamb, 1932; Ball, 1965). The observed 90 h oscillation period is somewhat shorter than the 123 h period of the free oscillation in a circular paraboloid, but near the 88 h period for a circular basin with a conical depth profile (Saylor *et al.*, 1980). Huang and Saylor (1982) went on to show that both a residual positive vorticity or the combination of the free mode and a forced topographic wave of higher frequency would tend to decrease the observed period of a free mode. As shown by Allender and Saylor (1979) at very low frequencies (<0.1 cpd), baroclinic effects are certainly important, but in the intermediate range (0.125–0.3 cpd), the barotropic oscillations appear to dominate.

Analytic models of the low-frequency barotropic response of lakes have been proposed by Birchfield (1967, 1969, 1972), Csanady (1973, 1976, 1978), Birchfield and Hickie (1977), and of course the classic works of Lamb (1932) and Ball (1965) on free oscillations of the second class in enclosed basins (also known as topographic Rossby waves or vortex modes). Huang and Saylor (1982) further investigated the response of the lowest free mode in an elliptic paraboloid to periodic forcing. All of these studies have shown that barotropic current fluctuations at frequencies much lower than the inertial frequency tend to be basically nondivergent. The important dynamic variable is potential vorticity, $\xi = f/D$ (where f is the Coriolis parameter and D is depth), and its gradient determines the structure and phase of the current oscillations. In the ocean, the variation of potential vorticity is due mainly to the variation of the Coriolis parameter with latitude, but in lakes, it is due mainly to topographic variations.

Perhaps the first numerical study emphasizing only the low-frequency barotropic response in lakes was that by Rao and Murty (1970). They examined the

[1] GLERL Contribution No. 357.

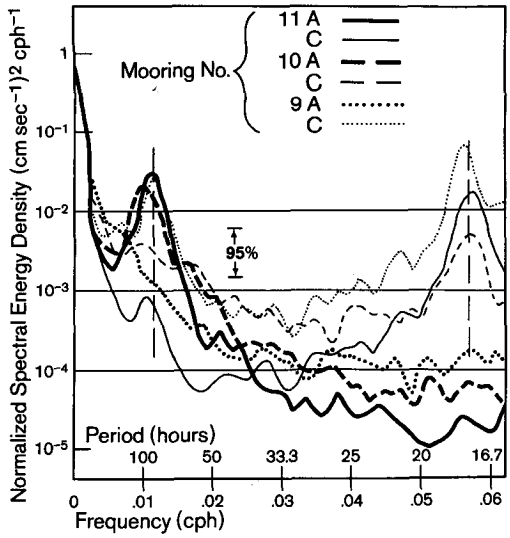

FIG. 1. Rotary spectra showing clockwise (C) and anticlockwise (A) components of low-frequency current oscillations in Lake Michigan in 1976. (From Saylor *et al.*, 1980.)

steady-state (zero-frequency) response of Lake Ontario, and later of the other Great Lakes (Murty and Rao, 1970), to constant wind stress by solving a discretized version of the barotropic vorticity equation on a numerical grid. The resulting circulation patterns were similar to the structure of the lowest topographic Rossby wave, generally consisting of two counterrotating gyres with flow in the direction of the wind near the shore and with return flow in deeper water. Allender (1977) compared results from three state-of-the-art baroclinic models and one barotropic model to currents observed in Lake Michigan during September 1963. Using a 10.8 km grid to represent the bathymetry of the lake, he found that the model currents were no better predictors of observed currents than a prediction of zero. Simons (1980) describes and summarizes numerous approaches to circulation modeling that include the effects of nonlinear terms, variable eddy viscosity, and stratification. However, in many natural systems the principal dynamics of low-frequency current fluctuations are linear, barotropic, and topographically controlled.

The main purpose of this paper is to determine whether a simple numerical model can simulate the observed low-frequency current oscillations in Lake Michigan in order to learn more about what really limits our ability to simulate currents in large lakes. Two models are tested. One is a quasi-linear, barotropic rigid-lid model that uses observed time-dependent wind forcing to simulate time-dependent current fluctuations. Model currents are found to compare reasonably well with observed currents only over a limited range of frequencies corresponding to the dominant forcing frequencies. This indicates that providing a more detailed description of the time- and space-dependent wind field may improve model results in this frequency range more than using a higher-order model. The second model assumes purely oscillatory wind forcing and determines the resulting oscillatory circulation pattern. This model is used to examine the spatial structure of the response of the lake as a function of forcing frequency in order to determine whether or not the model exhibits any peaks in the average kinetic-energy spectrum that would indicate the existence of whole-basin topographic modes. Results indicate that, for realistic values of bottom friction, the average response of the lake does not show any resonant peaks at low frequencies.

2. Time-dependent model

The time-dependent rigid-lid model is based on the barotropic vorticity equation

$$\frac{\partial}{\partial t}(\nabla \cdot \mathbf{D}^{-1}\nabla\psi) + J(\psi, \xi) = \mathbf{k} \cdot \mathrm{curl}\left(\frac{\tau_S - \tau_B}{\rho D}\right), \quad (1)$$

where ψ is the stream function, D depth, f the Coriolis parameter (10^{-4} rad s^{-1} for Lake Michigan), τ_S surface stress, τ_B bottom stress, $\mathbf{k}$ a vertical unit vector, J the Jacobian operator

$$J(\psi, \xi) = \frac{\partial\psi}{\partial x}\frac{\partial\xi}{\partial y} - \frac{\partial\psi}{\partial y}\frac{\partial\xi}{\partial x}, \quad (2)$$

and $\xi = f/D$ is potential vorticity. The lateral boundary condition for an enclosed basin,

$$\psi = 0 \quad \text{on the boundary}, \quad (3)$$

guarantees that there is no mass transport normal to the shoreline. Nonlinear acceleration and horizontal diffusion of momentum have been neglected in comparison to first-order acceleration and Coriolis terms. This simple framework has been used widely in numerical circulation models. [See Simons (1980) for a review of several models.]

Schwab *et al.* (1981) describe one possible numerical scheme to solve Eq. (1). The scheme is quasi-linear in that bottom friction is taken as

$$\rho^{-1}\tau_B = C_D|\bar{\mathbf{v}}|\mathbf{v}, \quad (4)$$

where $\mathbf{v} = (u, v)$ is the velocity vector defined by

$$u = \frac{-1}{D}\frac{\partial\psi}{\partial y}, \quad v = \frac{1}{D}\frac{\partial\psi}{\partial x}, \quad (5)$$

and C_D is a constant drag coefficient. However, in the numerical time stepping procedure, $|\bar{\mathbf{v}}|$ is calculated from ψ at the previous time step, while $\mathbf{v}$ is taken as the average of the previous and current timesteps. Arakawa's (1970) method is used to evaluate the Jacobian term:

$$12\Delta s^2 J(\psi, \xi) = \psi_{i+1,j}(\xi_{i,j+1} + \xi_{i+1,j+1} - \xi_{i,j-1} - \xi_{i+1,j-1})$$

$$+ \psi_{i-1,j}(-\xi_{i,j+1} - \xi_{i-1,j+1} + \xi_{i,j-1} + \xi_{i-1,j-1})$$
$$+ \psi_{i,j+1}(-\xi_{i+1,j} - \xi_{i+1,j+1} + \xi_{i-1,j} + \xi_{i-1,j+1})$$
$$+ \psi_{i,j-1}(\xi_{i+1,j} + \xi_{i+1,j-1} - \xi_{i-1,j} - \xi_{i-1,j-1})$$
$$+ \psi_{i+1,j+1}(-\xi_{i+1,j} + \xi_{i,j+1})$$
$$+ \psi_{i+1,j-1}(\xi_{i+1,j} - \xi_{i,j-1})$$
$$+ \psi_{i-1,j+1}(\xi_{i-1,j} - \xi_{i,j+1})$$
$$+ \psi_{i-1,j-1}(-\xi_{i-1,j} + \xi_{i,j-1}), \quad (6)$$

where ψ is averaged over the previous and current time step and the subscripts denote grid indices of the discretized variables. The grid interval is Δs and $\psi_{i,j}$ is defined at the upper right corner of grid square i, j. The time derivative in Eq. (1) is represented as a centered difference and all other spatial derivatives are replaced with elementary second-order differences. The resulting implicit system of equations is solved by overrelaxation at each time step. Schwab *et al.* (1981) show that there are two practical limits on the time step Δt. First,

$$\Delta t \leq 1.5/f \quad (7)$$

to ensure that the system of equations at each time step remains well-conditioned and second,

$$\Delta t \leq \min\left(\frac{2D}{C_D|\mathbf{v}|}\right) \quad (8)$$

to prevent spurious $2\Delta t$ oscillations in the current field. More details of the numerical method and a complete program listing are given by Schwab *et al.* (1981).

Wind stress is determined at each time step from observations of wind speed and direction and from air temperature at six weather stations around Lake Michigan. Overland wind is converted to an appropriate overwater wind using the formulas

$$U_w = U_L\left(1.2 + \frac{1.85}{U_L}\right)\left(1 - \frac{\Delta T}{|\Delta T|}\left|\frac{\Delta T}{1920}\right|^{1/3}\right), \quad (9)$$

$$\Delta\theta = (12.5 - 1.5\Delta T) - (0.38 - 0.03\Delta T)U_w, \quad (10)$$

where U_w and U_L are overwater and overland wind speed (m s^{-1}), ΔT is air temperature minus water temperature (°C), and $\Delta\theta$ is the clockwise angle between overland and overwater wind (deg). These formulas are based on graphs developed by Resio and Vincent (1977). Schwab and Morton (1983) showed that Eq. (9) resulted in a 2 m s^{-1} rms difference between estimated overwater wind speed and wind speed observed at buoys in Lake Erie as compared to a 2.6 m s^{-1} difference between raw overland and overwater wind speed and that this was close to the minimum difference that could be obtained by a simple empirical formula. With $\Delta T = 0$, Eq. (10) gives 10.6° veering to a 5 m s^{-1} wind and 8.7° veering to a 10 m s^{-1} wind, reasonable values for neutral-stability conditions. When applying Eqs. (9) and (10), surface-water temperature was taken from the climatological curve presented by Feit and Goldenberg (1976) for southern Lake Huron since no such curve was available for Lake Michigan. Overwater winds are then converted to surface stresses by a procedure described by Schwab *et al.* (1981). The method is based on Charnock's (1955) formula for roughness length over water and the Businger *et al.* (1971) formula for stability length. The constant in Charnock's formula is chosen so that the bulk aerodynamic transfer coefficient for momentum is 1.62×10^{-3} for neutral stability ($\Delta T = 0$) and a wind speed of 15 m s^{-1} at 10 m height. The spatial variability of surface stress is then assumed to be linear in x and y, i.e.,

$$\rho^{-1}\tau_s^x = a_1(t)x + b_1(t)y + c_1(t) \quad (11)$$

$$\rho^{-1}\tau_s^y = a_2(t)x + b_2(t)y + c_2(t), \quad (12)$$

where the coefficients $a_1, \ldots, c_2$ are determined by least-squares fitting to the six weather stations. This interpolation method is easy to implement computationally and still allows for a first-order curl in the wind stress field.

3. Oscillatory forcing model

If we assume periodically varying wind stress and streamfunction

$$\tau_s = \hat{\tau}_s(x, y)e^{i\omega t}, \quad \psi = \hat{\psi}(x, y)e^{i\omega t}, \quad (13)$$

where $\hat{\tau}$ and $\hat{\psi}$ are complex quantities, Eq. (1) becomes

$$i\omega\nabla\cdot\mathbf{D}^{-1}\nabla\hat{\psi} + J(\hat{\psi}, \xi) = \mathbf{k}\cdot\mathrm{curl}\left(\frac{\hat{\tau}_s - \hat{\tau}_B}{\rho D}\right). \quad (14)$$

The real part of $\hat{\psi}e^{i\omega t}$ then determines the circulation pattern at time t, i.e.,

$$\mathrm{Re}(\hat{\psi}e^{i\omega t}) = \hat{\psi}^R\cos\omega t - \hat{\psi}^I\sin\omega t. \quad (15)$$

Bottom friction is linearized in the oscillatory forcing model as

$$\rho^{-1}\tau_B = \frac{C_D S\mathbf{v}}{D}, \quad (16)$$

where S may be a function of x and y but not t. As Platzman (1963) showed, Eq. (16) represents the shallow water limit of Ekman theory with constant eddy viscosity coefficient ν if we define

$$S = 2.5\nu/C_D. \quad (17)$$

Eq. (14) is a generalization of the steady-state ($\omega = 0$) model proposed by Rao and Murty (1970) to arbitrary frequency. The method of solution is by relaxation; however, some care must be taken in the details of the numerical procedure. The relaxation procedure uses the discretized version of Eq. (14) with the Jacobian given by Eq. (16). $\hat{\psi}_{i,j}$ is isolated on the

left side of Eq. (14) and renamed $\hat{\psi}'_{i,j}$. Then the new value of $\hat{\psi}'_{i,j}$ in the iteration procedure is given by

$$\hat{\psi}^{\text{new}}_{i,j} = \hat{\psi}_{i,j} + r(\hat{\psi}'_{i,j} - \hat{\psi}_{i,j}). \tag{18}$$

Here r is the relaxation factor. Eq. (18) is first applied at all grid points for which $i + j$ is even. Then the procedure is applied to points for which $i + j$ is odd. This hopscotch technique was found to be necessary for convergence of the scheme. In addition, the relaxation parameter, r, is defined as a complex number. At high values of ω ($\omega > f/4$), a purely real overrelaxation factor could be used, but at lower values of ω, convergence was only achieved with complex values of the relaxation parameter. Typical values of the relaxation parameter for the 5 km Lake Michigan grid with S = constant = 2.5 m^2 s^{-1} are given in Table 1. Convergence of the scheme was assumed when

$$\frac{\max(|\hat{\psi}' - \hat{\psi}|)}{\max(\hat{\psi}^R, \hat{\psi}^I) - \min(\hat{\psi}^R, \hat{\psi}^I)} \leq 10^{-3}, \tag{19}$$

where max and min mean the maximum and minimum over all grid points.

4. Results

a. Time-dependent model

The time-dependent model was implemented on the 5 km square grid of Lake Michigan shown in Fig. 2. Regions of the lake shallower than 12.5 m were eliminated from the grid. Islands were also eliminated and replaced with 13 m water depth. The resulting grid contained 2093 squares with an average depth of 90.6 m. For the time-dependent model, the bottom drag coefficient was taken as 0.002. Three-hourly winds and temperatures from the six weather stations shown in Fig. 2 were obtained for April–November 1976. The average values of the coefficients $a_1, \ldots, c_2$ in Eqs. (11)–(12) for the 8-month period were

$$\left.\begin{aligned} a_1 &= 1.1 \times 10^{-11}\ \text{m s}^{-2}, \quad a_2 = 3.2 \times 10^{-11}\ \text{m s}^{-2} \\ b_1 &= 7.1 \times 10^{-12}\ \text{m s}^{-2}, \quad b_2 = -6.7 \times 10^{-12}\ \text{m s}^{-2} \\ c_1 &= 1.2 \times 10^{-5}\ \text{m}^2\ \text{s}^{-2}, \quad c_2 = -8.4 \times 10^{-6}\ \text{m}^2\ \text{s}^{-2} \end{aligned}\right\},$$

TABLE 1. Relaxation parameters used for Lake Michigan 5 km grid oscillatory-forcing model.

	Relaxation parameter	
ω/f	Real part	Imaginary part
0	0.075	0
0.0625	0.25	0.36
0.0750	0.36	0.45
0.0875	0.50	0.50
0.1000	0.60	0.60
0.1125	0.75	0.55
0.125–0.25	1.0	0.5
0.25–1	1.6	0

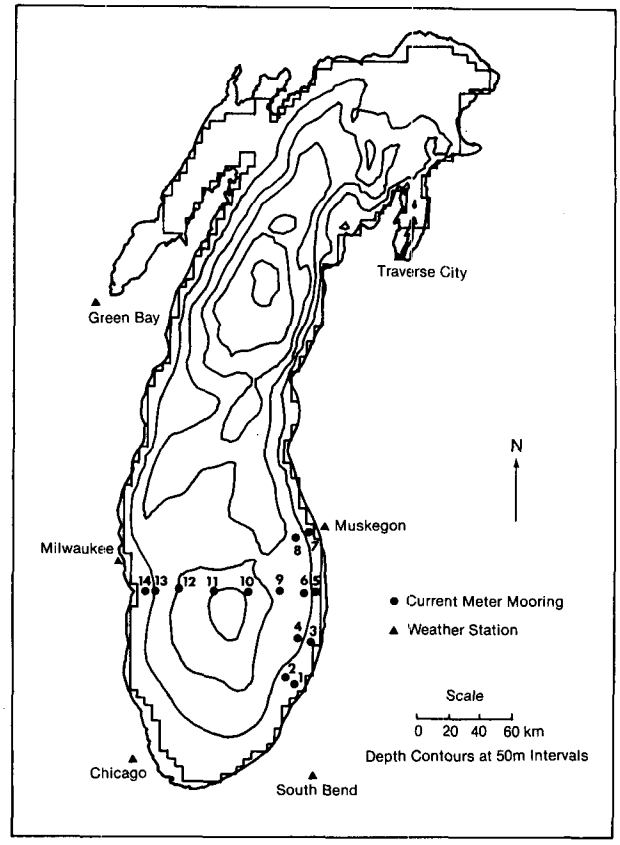

FIG. 2. Weather station locations, current-meter moorings, and 5 km computational grid for Lake Michigan.

implying a mean stress direction of WNW, a net cyclonic vorticity, and a positive net divergence. The time-dependent model was run with Δt = 2 h and the computed stream function fields were saved for further analysis.

Also shown in Fig. 2 are the current meter mooring locations used by Saylor *et al.* (1980). Most moorings consisted of a shallow (12.5 m) and a deep (25 m) AMF vector-averaging current meter. Some of the deeper moorings also had a current meter at 50 m. The current meters were deployed in May 1976 and recovered the following November.

Time series of model currents at the grid square nearest each current meter mooring were obtained at 8 h intervals from the calculated streamfunction field by averaging the values of u and v as defined in Eq. (5) from the left and right sides of the grid box for u or the upper and lower sides for v. A statistical comparison of observed and modeled currents is given in Table 2. The 8 h time series of observed currents were filtered to remove energy at frequencies greater than 0.5 cpd (48 h period) and compared to model currents in terms of Fourier norms (rms differences) and angle differences in order to compare the results to those of Allender (1977). The Fourier norm of $\mathbf{v}_1$ and $\mathbf{v}_2$ is defined as

TABLE 2. Statistical comparison of observed ($\mathbf{v}_o$) and computed ($\mathbf{v}_c$) current vectors. Observed currents have been filtered to remove energy at frequencies > 0.5 cpd.

Mooring no.	Depth (m)	$\|\mathbf{v}_o, 0\|$ (cm s^{-1})	$\|0, \mathbf{v}_c\|$ (cm s^{-1})	$\|\mathbf{v}_o, \mathbf{v}_c\|$ (cm s^{-1})	$\langle\Delta\theta\rangle$	$\dfrac{\|\mathbf{v}_o, \mathbf{v}_c\|}{\|\mathbf{v}_o, 0\|}$
2	12.5	8.24	3.93	7.81	0.46	0.95
3	12.5	11.75	8.41	9.83	0.40	0.84
4	12.5	7.19	5.78	6.36	0.40	0.88
4	25.0	6.54	5.78	5.23	0.36	0.80
5	12.5	12.94	5.00	11.81	0.37	0.91
5	25.0	10.50	4.99	8.29	0.30	0.79
6	12.5	6.79	3.41	5.64	0.34	0.83
6	25.0	6.11	3.41	4.86	0.34	0.80
7	12.5	10.29	6.94	8.63	0.33	0.84
8	12.5	9.30	4.40	7.81	0.39	0.84
8	25.0	8.61	4.40	6.97	0.40	0.81
9	12.5	5.49	2.41	4.99	0.39	0.91
9	25.0	4.79	2.41	4.14	0.38	0.87
9	50.0	4.87	2.41	4.00	0.37	0.82
11	32.5	4.34	2.11	4.18	0.44	0.96
11	70.0	3.52	2.11	3.55	0.44	1.01
12	25.0	5.85	2.26	5.40	0.37	0.92
12	50.0	5.37	2.26	4.79	0.36	0.89
13	25.0	9.76	4.82	8.14	0.33	0.83
14	25.0	9.83	8.13	9.06	0.33	0.92
10	28.0	4.57	2.55	4.32	0.39	0.95
10	40.5	4.56	2.55	4.30	0.39	0.94

$$\|\mathbf{v}_1, \mathbf{v}_2\| = \left(\frac{1}{M}\sum_{t=\Delta t}^{M\Delta t} |\mathbf{v}_1 - \mathbf{v}_2|^2\right)^{1/2} \tag{20}$$

and the average angle difference as

$$\langle\Delta\theta\rangle = \frac{1}{\pi M}\sum_{t=\Delta t}^{M\Delta t} \cos^{-1}\left(\frac{\mathbf{v}_1 \cdot \mathbf{v}_2}{|\mathbf{v}_1||\mathbf{v}_2|}\right), \tag{21}$$

so that a value of $\langle\Delta\theta\rangle = 0$ implies perfect directional agreement. The values of average angle difference and $\|\mathbf{v}_o, \mathbf{v}_c\|/\|\mathbf{v}_o, 0\|$ are somewhat better than those reported by Allender (1977) for currents obtained with a multilayer baroclinic model averaging 0.38 for angle difference and 0.88 for $\|\mathbf{v}_o, \mathbf{v}_c\|/\|\mathbf{v}_o, 0\|$, compared to Allender's values of 0.39–0.45 for angle difference and 1.00–1.11 for $\|\mathbf{v}_o, \mathbf{v}_c\|/\|\mathbf{v}_o, 0\|$.

For comparison, Table 3 gives the Fourier norms and average angle differences between low-pass filtered observed currents at the five pairs of nearshore moorings and at two different depths on moorings 5 and 6. The differences between current-meter moorings separated by less than 10 km and even between currents at different depths on the same mooring are comparable to the differences between the observed and computed currents. The comparison between the nearshore moorings is somewhat deceiving in that, although the moorings are not very far apart, the water depth differs by as much as 20 m, but this difference is only slightly greater than the difference between grid-square centers and actual mooring locations. Note also that the values of $\|\mathbf{v}_a, \mathbf{v}_b\|/\|0, \mathbf{v}_b\|$ would be considerably greater than $\|\mathbf{v}_a, \mathbf{v}_b\|/\|\mathbf{v}_a, 0\|$. And as with all calculations of Fourier norms, small phase differences between time series can give large error norms.

From Table 2, we can also calculate the multiplicative factor, C, for computed currents that would minimize the overall Fourier error norm $\Sigma\, \|\mathbf{v}_o, C\mathbf{v}_c\|$. This value is given by

$$C = \frac{\sum (\|\mathbf{v}_o, 0\|^2 + \|0, \mathbf{v}_c\|^2 - \|\mathbf{v}_o, \mathbf{v}_c\|^2)}{2\sum \|0, \mathbf{v}_c\|^2}. \tag{22}$$

The numerical value of C is 0.87 and the overall error norm is 6.71 cm s^{-1}. However, the average energy of the computed currents is less than the energy of the observed currents by a factor of 2.96, suggesting that the magnitude of the computed currents should be increased by a factor of 1.72. For $C = 1.72$, the overall error norm is increased by 15% to 7.74 cm s^{-1}.

Figure 3 shows a typical vector time series plot of computed and observed (low-pass filtered) currents from mooring 5. The observed currents are from 25 m. The plots begin on 1 April 1976. Many of the oscillatory features of the observed currents are reproduced by the model, but the magnitude of the computed currents is generally lower than that of the observed currents. Some features in the observed currents, like the 10 days of southward flow starting on day 75, are missed completely by the model.

At stations away from shore, the vector time series plots are difficult to compare since currents tend to be more omnidirectional. The progressive-vector diagram

TABLE 3. Statistical comparison of low-pass filtered observed currents.

Mooring a	Depth (m)	Mooring b	Depth (m)	Separation distance (km)	$\|\mathbf{v}_a, 0\|$ (cm s^{-1})	$\|0, \mathbf{v}_b\|$ (cm s^{-1})	$\|\mathbf{v}_a, \mathbf{v}_b\|$ (cm s^{-1})	$\langle\Delta\theta\rangle$	$\dfrac{\|\mathbf{v}_a, \mathbf{v}_b\|}{\|\mathbf{v}_a, 0\|}$
3	12.5	4	12.5	7.7	11.75	7.19	8.77	0.31	0.75
5	12.5	6	12.5	8.2	12.94	6.79	12.29	0.42	0.95
5	25.0	6	25.0	8.2	10.50	6.11	8.99	0.34	0.86
7	12.5	8	12.5	7.6	10.29	9.30	9.62	0.35	0.93
13	25.0	14	12.5	6.5	9.76	9.83	10.91	0.38	0.12
5	12.5	5	25.0	0	12.94	10.50	9.56	0.24	0.74
6	12.5	6	25.0	0	6.79	6.11	4.13	0.23	0.61

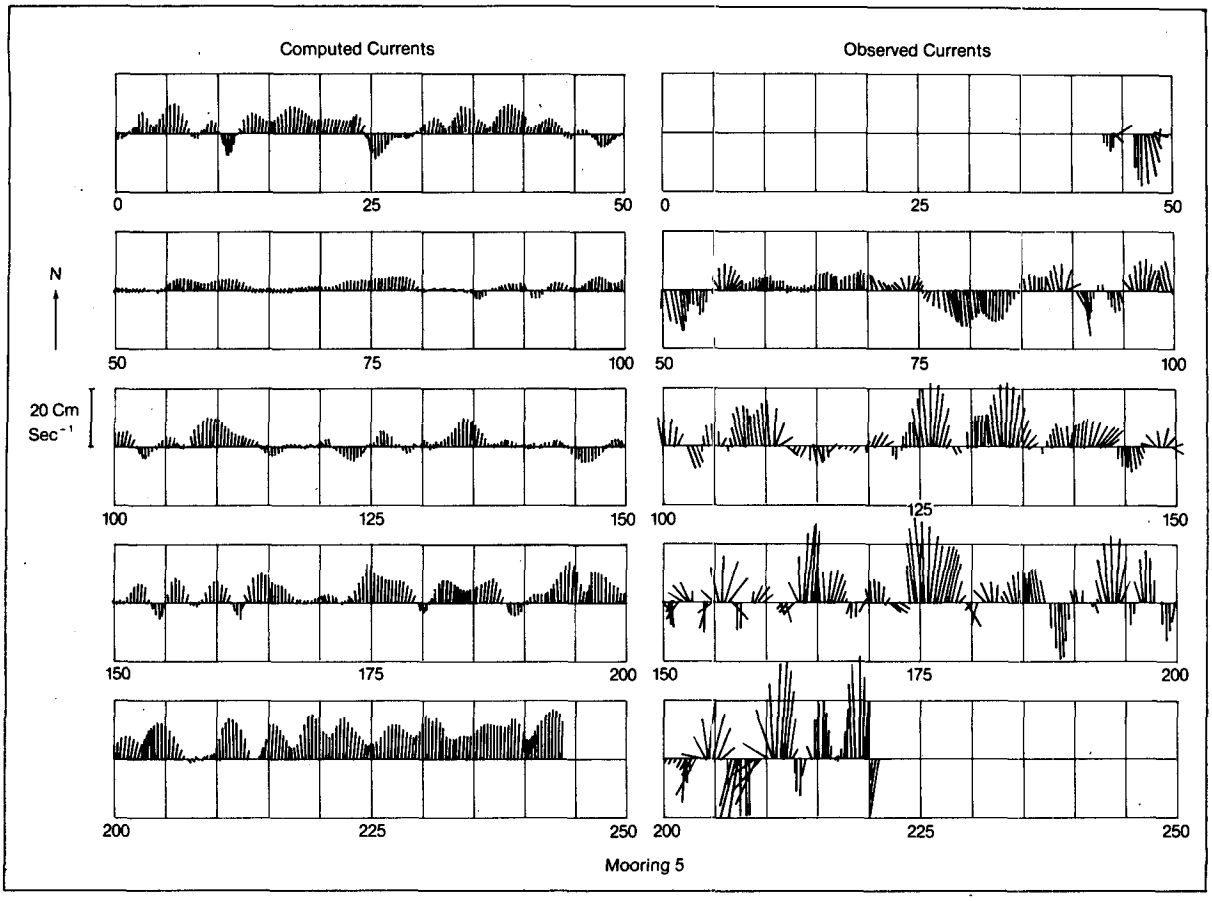

FIG. 3. Vector time series of computed (left panel) and observed (right panel) currents at mooring 5 in Lake Michigan. Time series start on 1 April 1976. Observed currents are from 25 m and have been low-pass filtered to remove energy at frequencies > 0.5 cpd.

is a more useful comparison tool here. Fig. 4 shows the progressive-vector diagrams of computed and observed (low-pass filtered at 28 m depth) currents at mooring 10 starting 1 July 1976 and continuing for 32 days. Again, the oscillatory features are similar. The modeled currents are in good phase agreement with

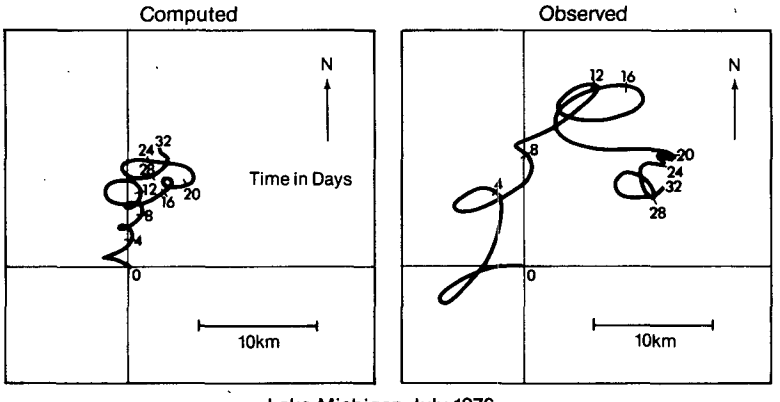

FIG. 4. Progressive-vector diagrams of computed (left) and observed (right) currents at mooring 10 in Lake Michigan. Indicated time is in days from 1 July 1976. Observed currents are from 28 m and have been low-pass filtered to remove energy at frequencies greater than 0.5 cpd.

observed currents at days 4, 8, 12 and 16, but the magnitude of the model currents is lower than that of the observed currents and the very-low-frequency component of the motion is not reproduced in the model.

Kinetic-energy spectra were calculated for 512-point subseries of the 8 h observed (unfiltered) and model currents starting on 14 May 1976. The spectra were calculated by averaging the magnitudes of the discrete Fourier transforms of 17 overlapping 256-point subsections of the original 512-point time series. Each subsection is tapered with a full cosine bell. There are 128 frequency bands each 0.0117 cpd wide, so the number of degrees of freedom for each energy spectrum is eight. The low-frequency portion of the average kinetic-energy spectrum for 22 current meters and for modeled currents at 15 points is shown in Fig. 5. Also shown is the spectrum of $\rho^{-1}\tau_s$ at a point corresponding to current-meter mooring 11 in the center of the southern basin. The 95% confidence interval for eight degrees of freedom is shown, although the average spectra have considerably higher reliability than this. Thin vertical lines emphasize certain peaks that appear in all three spectra. At frequencies greater than 0.6 cpd, the kinetic energy of the model currents continues to drop, while the kinetic energy of the observed currents begins to rise to a peak at the inertial frequency (1.38 cpd).

From Fig. 5 it is clear that the average energy of the computed currents is less than that of the observed currents, but in the frequency range 0.125–0.3 cpd, the energy values are closer. This frequency range corresponds to the broad maximum in the wind-stress spectrum. At very low frequencies (<0.1 cpd), the model currents grossly underestimate the kinetic energy of the observed currents.

b. *Oscillatory-forcing model*

The oscillatory-forcing model described in the previous section was run on the same 5 km grid of Lake Michigan as the time-dependent model for the forcing frequencies given in Table 1. For $0.125 \leqslant \omega/f < 0.25$, the step in ω/f was 0.005. For $0.25 \leqslant \omega/f \leqslant 1$, the step was 0.025. The magnitude of the wind stress was 1 dyn cm^{-2}. Only north–south oscillations were considered because, as Pickett (1980) pointed out, much more energy is imparted to the circulation pattern from winds parallel to the major axis of a lake than from cross winds. The linear bottom friction coefficient S defined in Eq. (16), can be thought of as a time-averaged value of the vertically integrated current. From the time-dependent model runs, it was found that time-averaged values of vertically integrated currents were in the range of 1–6 m^2 s^{-1}, so S was taken as a constant 2.5 m^2 s^{-1}.

For each value of the forcing frequency, the total kinetic energy of the resulting circulation pattern was calculated as

$$\mathrm{TKE} = \frac{\rho}{2T}\int\int D|\mathbf{v}_c|^2 dA dt = \frac{\rho}{4}\int D^{-1}\left(\left|\frac{\partial\hat{\psi}}{\partial x}\right|^2 + \left|\frac{\partial\hat{\psi}}{\partial y}\right|^2\right)dA, \quad (23)$$

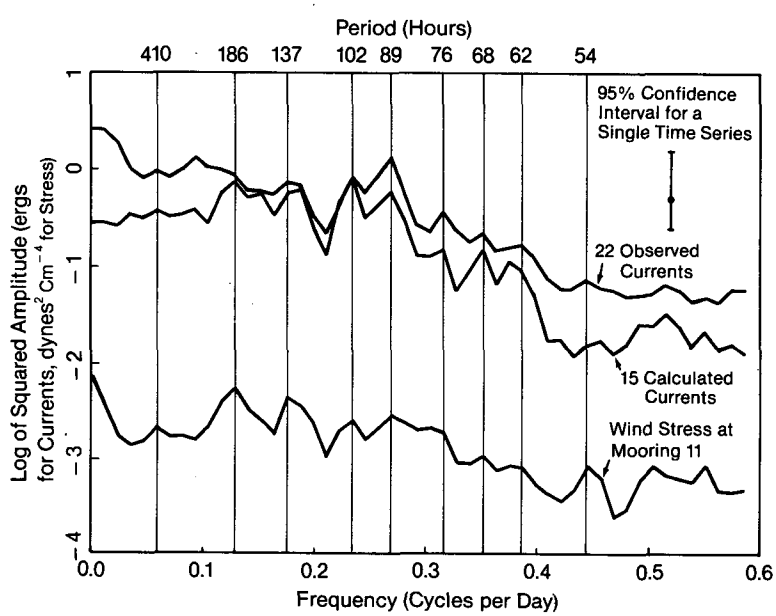

FIG. 5. Low-frequency part of average kinetic-energy spectra of observed currents, calculated currents, and wind stress in Lake Michigan, May–October 1976. Vertical lines labeled with corresponding period in hours indicate peaks that appear in all three spectra.

where the time integral is taken over one oscillation period, $T = 2\pi/\omega$. The plot of total kinetic energy versus forcing frequency is shown in Fig. 6. Over the entire range of forcing frequencies tested, there is no evidence of any resonant response. This is consistent with the results of the time-dependent model shown in Fig. 5, where all the peaks in the energy spectrum of computed currents correspond to peaks in the forcing spectrum. If friction were lowered, presumably at some point resonant peaks would appear in the oscillatory-forcing-model kinetic-energy spectrum at the frequencies of the free topographic modes of oscillation, but for the conservatively low value of the friction parameter used here, the response is nonresonant at all frequencies.

One purpose of this investigation was to model the spatial structure of the low-frequency response of Lake Michigan. The oscillatory-forcing-model results show that over the frequency range 0.125–0.3 cpd the spatial structure of the response of the lake to oscillatory forcing is almost independent of frequency. Figs. 7 and 8 show the streamfunction pattern and wind stress vector at one-sixteenth-period intervals for forcing frequencies 0.15 and 0.25 cpd. Only half a cycle is shown since the other half cycle is symmetric. In the southern part of the lake, the response consists of two counterrotating gyres, similar to the pattern one would expect for a free topographic wave. The phase of the gyres in relation to the wind is such that the maximum return current in the center of the southern basin occurs one-eighth to one-quarter period after the maximum wind stress. The northern part of the lake exhibits a simple two-gyre pattern only between one- and three-eighths of a period after the maximum wind stress. In the intervening time, the pattern is very complicated. The similarity of the circulation pattern to a free wave extends to the counterclockwise rotation of the gyres around the southern basin.

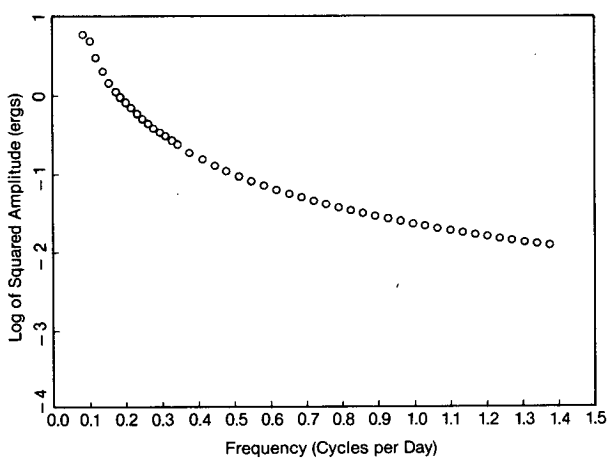

FIG. 6. Lakewide average kinetic energy in Lake Michigan as a function of forcing frequency.

At frequencies < 0.125 cpd, the circulation patterns tend to become more complicated, with increasingly narrower boundary layers along the east and west shores of the lake. The steady-state (zero-frequency) response to a 1 dyn cm^{-2} southerly wind is shown in Fig. 9. The boundary layer structure is apparent. The structure is similar to Birchfield's (1967) analytic solution for a circular basin, with Ekman flow to the right of the wind in the deeper parts of the lake. There is a swift, jet-like structure near the shore. The numerical results of Murty and Rao (1970) for steady-state circulation in Lake Michigan showed a much simpler pattern, with basically two circulation cells elongated in the north–south direction. Flow in the deep parts of the lake was directly against the wind. The maximum amplitude of the stream function in Fig. 9 is 3.6×10^5 m^3 s^{-1}, while Murty and Rao's solution has a maximum amplitude of $\sim 4\times 10^4$ m^3 s^{-1}. Murty and Rao (1970) used a slightly different parameterization of bottom friction than in the oscillatory-forcing model, namely

$$\rho^{-1}\tau_B = C_D|\bar{\mathbf{v}}|\mathbf{v}, \tag{24}$$

where $|\bar{\mathbf{v}}|$ is a constant average velocity. Comparing Eqs. (24) and (16), we have $|\bar{\mathbf{v}}| = S/D$ or $|\bar{\mathbf{v}}| = 2.5$ cm s^{-1} for $D = 100$ m, with $S = 2.5$ m^2 s^{-1} and $C_D = 0.002$. Murty and Rao quoted a value $|\bar{\mathbf{v}}| = 5$ cm s^{-1}, but the oscillatory forcing model was only able to reproduce the magnitude and structure of their circulation pattern for a south wind with $S = 100$ m^2 s^{-1} or $|\bar{\mathbf{v}}| = 100$ cm s^{-1} for $D = 100$ m. Clearly, this is unrealistic. Fig. 9 is in better agreement with known analytic solutions for comparable values of bottom friction.

5. Discussion and conclusions

The results of the time-dependent barotropic model for April–November 1976 agree reasonably well with observed currents in the 0.125–0.3 cpd frequency range. Comparison of observed and computed currents in terms of vector time series and progressive-vector diagrams indicates that the main oscillatory features of the observed currents with time scales of 3–8 days are reproduced fairly well. Statistical comparisons between observed and computed currents are slightly better than those observed by Allender (1977) with a multilayer baroclinic model for the month of September 1963. The differences are comparable to the differences between currents observed at nearby moorings or even at different depths at the same mooring. These results are somewhat surprising in that the lake is well stratified from July to October. Apparently, in the main wind-forcing frequency range, the overall response of the lake is primarily barotropic.

The principal remaining differences between computed and observed currents are that very-low-frequency fluctuations (<0.1 cpd) are not present in the

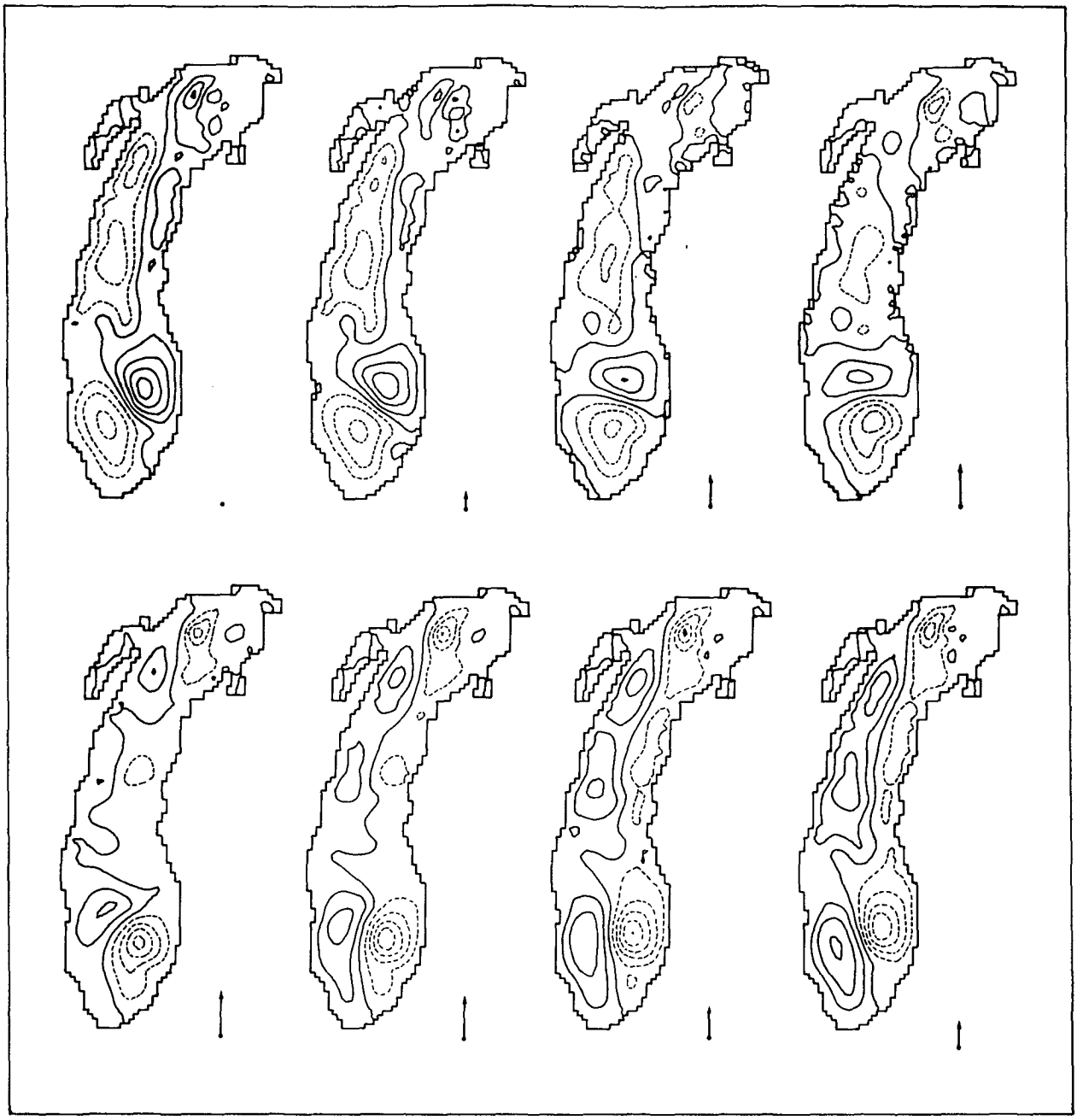

FIG. 7. Response of Lake Michigan to 0.15 cpd (160 h) periodic north–south forcing with amplitude 1 dyn cm^{-2} at one-sixteenth-period intervals. Streamlines are in increments of 4×10^4 m^3 s^{-1}. Dashed lines indicate negative streamfunction.

model results, the low-frequency fluctuations (3–8 day periods) have a slightly lower amplitude than the observed fluctuations, and inertial oscillations are not present in the model. The first two of these remaining differences bear further discussion. The third is expected, since the model is only applicable to barotropic fluctuations with time scales greater than two or three inertial periods and inertial oscillations are purely a result of baroclinicity.

The difference in observed and computed amplitudes in the main (3- to 8-day period) forcing band is not considered a serious shortcoming. Underestimation of overwater wind speed with Eq. (9), underestimation of drag coefficients, or underestimation of local overwater wind stress by the linear interpolation formulas Eqs. (11) and (12) could easily account for the difference. In addition, the computed currents are vertical averages, while the observations are made at a

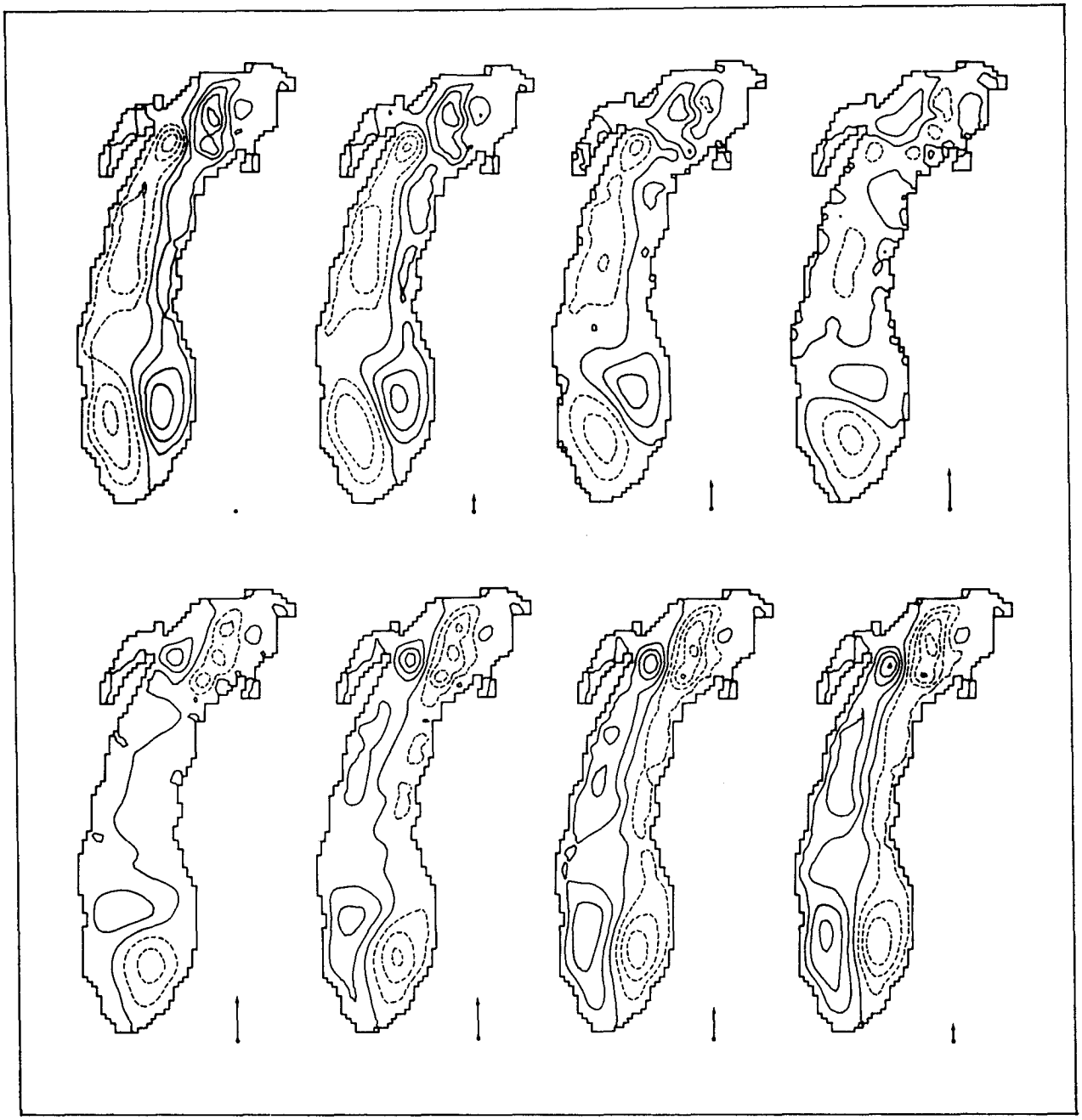

FIG. 8. Response of Lake Michigan to 0.25 cpd (100 h) periodic north–south forcing with amplitude 1 dyne cm^{-2} at one-sixteenth-period intervals. Streamlines are in increments of 2×10^4 m^3 s^{-1}. Dashed lines indicate negative stream function.

single point in the water column. Even though the statistical results of Table 2 suggest that the magnitude of the computed currents should be decreased to minimize the overall error norm, it is suggested that, when using the results of a vertically integrated barotropic model with similar forcing data for simulating the transport of particles or dissolved substances, the model currents should be increased by a factor of 1.5–2. It is more important for these simulations that the computed currents have the right energy than that they have the minimum error norm.

The considerably lower energy of the very-low-frequency (<0.1 cpd) fluctuations in the model currents is a more serious concern. The most likely explanation is that the model is barotropic and that low-frequency baroclinic motion accounts for the differences. In a study of monthly averages of the same Lake Michigan current meter data used here, Allender and Saylor

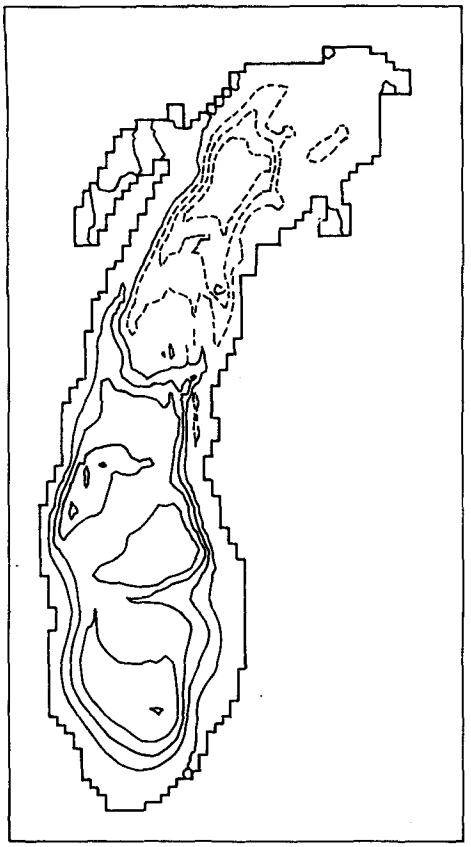

FIG. 9. Steady-state (zero frequency) response of Lake Michigan to northward 1 dyn cm^{-2} forcing. Streamlines are in increments of 8×10^4 m^3 s^{-1}. Dashed lines indicate negative stream function.

(1979) did in fact find evidence of vertical shear in the mean currents. It is difficult to find direct evidence of low-frequency baroclinic motion in the observed currents in that, over the longer time scales involved, the depth of the thermocline can change considerably. At moorings where simultaneous currents are available from above and below the thermocline, it does appear that there is more vertical shear in the very-low-frequency fluctuations than in the main wind-forcing band.

Another possible reason for the differences at very low frequencies is the limited grid resolution of the models. As results from the oscillatory-forcing model showed, the response of the lake in the frequency range 0.125–0.3 cpd had a fairly simple spatial structure, but at lower frequencies, the circulation pattern developed a boundary-layer character. Perhaps at very low frequencies, the 5 km grid resolution is not sufficient to resolve the spatial structure of even the barotropic response.

A third reason for the differences at low frequencies could be the neglect of nonlinear terms in the model. Nonlinear terms could provide a mechanism for leakage of energy from the main forcing frequency band to higher and lower frequencies as observed by Bennett and Magnell (1979). In their study, the nonlinearity was due mainly to bottom friction, but in Lake Michigan the nonlinear acceleration terms would probably be more important in providing a pathway for energy leakage. All three of these possibilities bear further investigation.

The oscillatory-forcing model showed that the average response of the lake to periodic, low-frequency forcing is nonresonant. The spatial structure of the response in the southern part of Lake Michigan is similar to the structure of the lowest topographic free oscillation in a circular basin. The rest of the lake has a two-gyre structure only during a portion of the forcing cycle. It appears that each bowl-shaped sub-basin of the lake sets up its own two-gyre response, with the relative phase and amplitude determined by the local topography. The whole-lake response may represent the combination of several free rotational modes, with nearby frequencies being forced simultaneously, so that no one single mode dominates. In an enclosed basin, there may be any number of rotational models in a given low-frequency range, so it may not be possible to calculate frequencies and structures of the modes explicitly. And, moreover, it may not be important to do so, since the forced response of the lake does not seem to favor any individual mode. Although the calculated steady (zero-frequency) response of the lake does not agree with the observed mean currents, it is consistent with previous analytic studies for steady circulation. Again, it would be very interesting to determine whether the difference is due to the effects of stratification, nonlinearity, grid resolution, or some other shortcoming of the model.

Acknowledgments. Dr. John R. Bennett was extremely helpful throughout the course of this work. Discussions with him led to several improvements in the time-dependent and oscillatory forcing model results. Dr. Bruce Warren and two reviewers provided valuable editorial suggestions.

REFERENCES

Allender, J. H., 1977: Comparison of model and observed currents in Lake Michigan. *J. Phys. Oceanogr.*, **7**, 711–718.

——, and J. H. Saylor, 1979: Model and observed circulation throughout the annual temperature cycle of Lake Michigan. *J. Phys. Oceanogr.*, **9**, 573–579.

Arakawa, A., 1970: Numerical simulation of large scale atmospheric motions. *Proc. of a Symp. in Applied Mathematics*, G. Birkhoff and S. Varga, Eds., Durham, N.C., Amer. Math. Soc., 24–40.

Ball, F. K., 1965: Second-class motions of a shallow liquid. *J. Fluid Mech.*, **23**, 545–561.

Bennett, J. R., and B. A. Magnell, 1979: A dynamical analysis of currents near the New Jersey coast. *J. Geophys. Res.*, **84**, 1165–1175.

Birchfield, G. E., 1967: Horizontal transport in a rotating basin of parabolic depth profile. *J. Geophys. Res.*, **72**, 6155–6163.

——, 1969: Response of a circular model Great Lake to a suddenly imposed wind stress. *J. Geophys. Res.*, **74**, 5547–5554.

——, 1972: Theoretical aspects of wind-driven currents in a sea or lake of variable depth with no horizontal mixing. *J. Phys. Oceanogr.*, **2**, 355–362.

——, and B. P. Hickie, 1977: The time-dependent response of a circular basin of variable depth to a wind stress. *J. Phys. Oceanogr.*, **7**, 691–701.

Businger, J. A., J. C. Wyngaard, Y. Izumi and E. F. Bradley, 1971: Flux-profile measurements in the atmospheric surface layer. *J. Atmos. Sci.*, **28**, 181–189.

Charnock, H., 1955: Wind stress on a water surface. *Quart. J. Roy. Meteor. Soc.*, **81**, 639.

Csanady, G. T., 1973: Wind-induced barotropic motions in long lakes. *J. Phys. Oceanogr.*, **3**, 429–438.

——, 1976: Topographic waves in Lake Ontario. *J. Phys. Oceanogr.*, **6**, 93–103.

——, 1978: The arrested topographic wave. *J. Phys. Oceanogr.*, **8**, 47–62.

Feit, D. M., and D. S. Goldenberg, 1976: Climatology of surface temperatures of Lakes Superior, Huron, Erie, and Ontario. U.S. Dept. of Commerce, NOAA, NWS, TDL, Office Note TDL-76-16, Silver Spring, Md., 14 pp.

Huang, J. C. K., and J. H. Saylor, 1982: Vorticity waves in a shallow basin. *Dyn. Atmos.-Oceans*, **6**, 177–196.

Lamb, H., 1932: *Hydrodynamics.* Dover, 738 pp.

Marmorino, G. O., 1979: Low-frequency current fluctuations in Lake Ontario, winter 1972–1973 (IFYGL). *J. Geophys. Res.*, **84**, 1206–1214.

Murty, T. S., and D. B. Rao, 1970: Wind-generated circulations in Lakes Erie, Huron, Michigan, and Superior. *Proc. Conf. Great Lakes Res., IAGLR*, **13**, 927–941.

Pickett, R. L., 1980: Observed and predicted Great Lakes winter circulations. *J. Phys. Oceanogr.*, **10**, 1140–1145.

Platzman, G. W., 1963: The dynamic prediction of wind tides on Lake Erie. *Meteor. Monogr.*, No. 26, Amer. Meteor. Soc., 44 pp.

Rao, D. B., and T. S. Murty, 1970: Calculation of the steady-state wind-driven circulations in Lake Ontario. *Arch. Meteor. Geophys. Bioklim.*, **A19**, 195–210.

Resio, D. T., and C. L. Vincent, 1977: Estimation of winds over the Great Lakes. *J. Waterway Port Coast. Ocean Div., ASCE*, **102**, 265–283.

Saylor, J. H., J. C. K. Huang and R. O. Reid, 1980: Vortex modes in southern Lake Michigan. *J. Phys. Oceanogr.*, **10**, 1814–1823.

Schwab, D. J., and J. A. Morton, 1983: Estimation of overlake wind speed from overland wind speed: A comparison of three methods. *J. Great Lakes Res.* (in press).

——, J. R. Bennett and A. T. Jessup, 1981: A two-dimensional lake circulation modeling system. NOAA Tech. Memo. ERL-GLERL-38, 79 pp.

Simons, T. J., 1980: Circulation models of lakes and inland seas. *Can. Bull. Fish. Aquatic Sci.*, **203**, 146 pp.